Engineering Structures 270 (2022) 114887

Contents lists available at ScienceDirect

Engineering Structures

journal homepage: www.elsevier.com/locate/engstruct

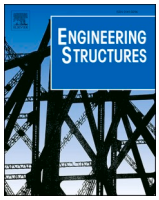

Experimental assessment of the monotonic and cyclic behaviour of exterior RC beam-column joints built with plain bars and non-seismically designed

José Melo [a,*], Humberto Varum [a], Tiziana Rossetto [b]

[a] CONSTRUCT-LESE, Faculty of Engineering (FEUP), University of Porto, Porto, Portugal
[b] EPICentre, University College London, London, UK

ARTICLE INFO

Keywords:
Existing RC structures
Exterior beam-column joints
Plain reinforcing bars
Full-scale tests
Cyclic behaviour

ABSTRACT

The seismic behaviour of reinforced concrete structures built with plain reinforcing bars is sometimes conditioned by the slippage between the reinforcing bars and the surrounding concrete in the elements as exterior beam-column joints. The anchorage of the beam reinforcing bars in the core joint with weak concrete confinement, inappropriate reinforcement detailing for seismic loads and poor bond properties are the common reasons for collapse of many structures. This paper presents the results of four unidirectional cyclic tests and two unidirectional monotonic tests carried out on full-scale exterior beam-column joints built with plain and deformed reinforcing bars. These specimens are representative of reinforced concrete structures built without adequate reinforcement detailing for seismic loads. The influence of bond properties, lapping of the longitudinal bars, anchorage of the beam reinforcing bars and loading on the beam-column joints response are investigated.

1. Introduction

Recent earthquakes have showed the vulnerability of the existing reinforced concrete (RC) structures to seismic loading, particularly the beam-column joints. Inappropriate joint reinforcement detailing may lead the structural elements to a premature failure, especially in the case of exterior beam-column joints. Typically, the failure mode in exterior joints with insufficient transverse reinforcement is concrete shear in the form of diagonal tension [1]. Slippage of the reinforcing bars can be another mechanism that may conditioned the seismic behaviour of the joints, especially in structures built with plain reinforcing bars and prior to the enforcement of the modern seismic-oriented designed codes. Cyclic loads such as those induced by earthquakes, cause progressive concrete-steel bond degradation, which can lead to significant bar slippage. As a result, the maximum strength capacity of the structure may not be reached and the elements' deformation might enlarge, leading to the premature collapse of the structure. The failure of old RC structures may be anticipated by other factors apart from bar slippage and weak joint confinement, such as [2]: inadequate reinforcement detailing for seismic demands; lower compressive concrete strength; and design only for gravity loads.

Depth research has developed on the design of new RC structures and improvement of design codes (for example [3–6]) but lower amount of studies have been focus on the assessment and retrofitting of old RC structures [7–20], and the cyclic behaviour of existing RC elements is not yet fully understood. The studies focus on the cyclic assessment of RC beams, columns and beam-column joints built with plain reinforcing bars [8–16], on the retrofitting of existing RC elements [9,17–20] and numerical modelling [7,14]. Recent studies also have focus on the retrofitting and strengthening of exterior RC beam-column joints with lack of shear reinforcement in the joint core and poor reinforcing detailing for seismic loading [21–24].

This paper describes an experimental campaign performed for assessment of the monotonic and cyclic behaviour of six full-scale RC exterior beam-column joints built with plain and deformed bars and without seismic reinforcement detailing. The specimens are representative of typical exterior beam-column joints in existing RC structures in the European Mediterranean countries built before the 70s. The influence of reinforcing steel surface, lap-splicing of longitudinal reinforcing bars, longitudinal beam reinforcing bars anchorage and lateral loading history (monotonic or cyclic) on the response are investigated.

The specimens were designed according to old RC codes and without seismic detailing in order to represent the typical exterior beam-column joint in existing RC buildings. Different reinforcement detailing was adopted in the specimens' design. An additional joint specimen built with deformed reinforcing bars was cyclically tested and the results

* Corresponding author.
E-mail address: josemelo@fe.up.pt (J. Melo).

https://doi.org/10.1016/j.engstruct.2022.114887
Received 6 January 2022; Received in revised form 26 July 2022; Accepted 22 August 2022
Available online 5 September 2022

were compared with an analogous specimen built with plain bars. The main results in terms of global and local response of this testing campaign are presented and discussed, allowing the study of the influence on the response of exterior beam-column joints of: bond properties; lapping of the longitudinal reinforcing bars on column; anchorage of the longitudinal beam reinforcing bars in the core joint; lateral loading (monotonic and cyclic); and joint shear strength prediction.

2. Specimens detailing, material properties and test setup

2.1. Detailing of joint specimens

The experimental campaign was performed in the Department of Civil Engineering at the University of Aveiro to describe the behaviour of existing exterior beam-column joints built with plain reinforcing bars under monotonic and cyclic loading. Five full-scale exterior beam-column joints were built with plain reinforcing bars and tested under lateral monotonic and cyclic loading until reach the rupture. Four specimens were design and detailed according to the first Portuguese codes for reinforcing concrete structures, RBA (1935) [25] and REBA (1967) [26], i.e. without shear reinforcement in the joint, without seismic detailing and not considering the more recent capacity design rules. Another specimen was built with poor anchorage (180° hooks) of the beam longitudinal reinforcement. An extra specimen was built with deformed reinforcing bars to study the influence of the bar surface on the response of the exterior beam-column specimens. All the specimens have inadequate shear transverse reinforcement detailing in the joint region in order to represent the typical existing RC structures designed only for gravity loads. The ratio between the moment of resistance of the columns and the moment of resistance of the beam is 0.8 and consequently the mechanism weak column-strong beam is observed.

The specimens represent exterior beam-column joints at the first-floor level of a four-storey building and connect beams with 4.0 m (157 in) span and columns with 3.0 m (118 in) height.

The geometry, dimensions, reinforcing details and nomenclature of the specimens are presented in Fig. 1. The cross-section dimensions are the same for all specimens being 0.25 × 0.25 m^2 (9.84 × 9.84 in^2) for columns and 0.25 × 0.40 m^2 (9.84 × 15.75 in^2) for beams. The anchorage of the longitudinal plain reinforcing bars consists in 180° end hooks except for specimens type TPA and TPB where the anchorage of the longitudinal reinforcing bars of the beam in the core joint consists in 90° bend followed by a straight length of 0.25 m (9.84 in) and ends with a 180° hook. The mandrel diameter and the straight prolongation after the hook are four times the bar diameter. In the specimen with deformed reinforcing bars 90° end hooks with a 0.15 m (5.9 in) and 0.30 m (11.8 in) straight prolongation after the hook were adopted for columns and beam, respectively. The lapping length of the longitudinal plain reinforcing bars is equal to 30 times the bar diameter and it was defined according to the recommendations of the first Portuguese RC codes. The stirrups were anchored by 90° bends in all specimens and the core joint did not have stirrups.

Specimens TPA-1 and TPA-2 have continuous longitudinal plain reinforcing bars. Specimen TPA-2 is assumed as reference specimen. Specimens TPB-1 and TPB-2 are similar to specimens TPA-1 and TPA-2 but with lap-splices in the longitudinal reinforcing bars located at the base of the superior column. Specimen TPC has continuous longitudinal plain reinforcing bars, but the reinforcing bars anchorage of the beam in the joint is made with 180° end hooks. Specimen TD is equivalent to TPA

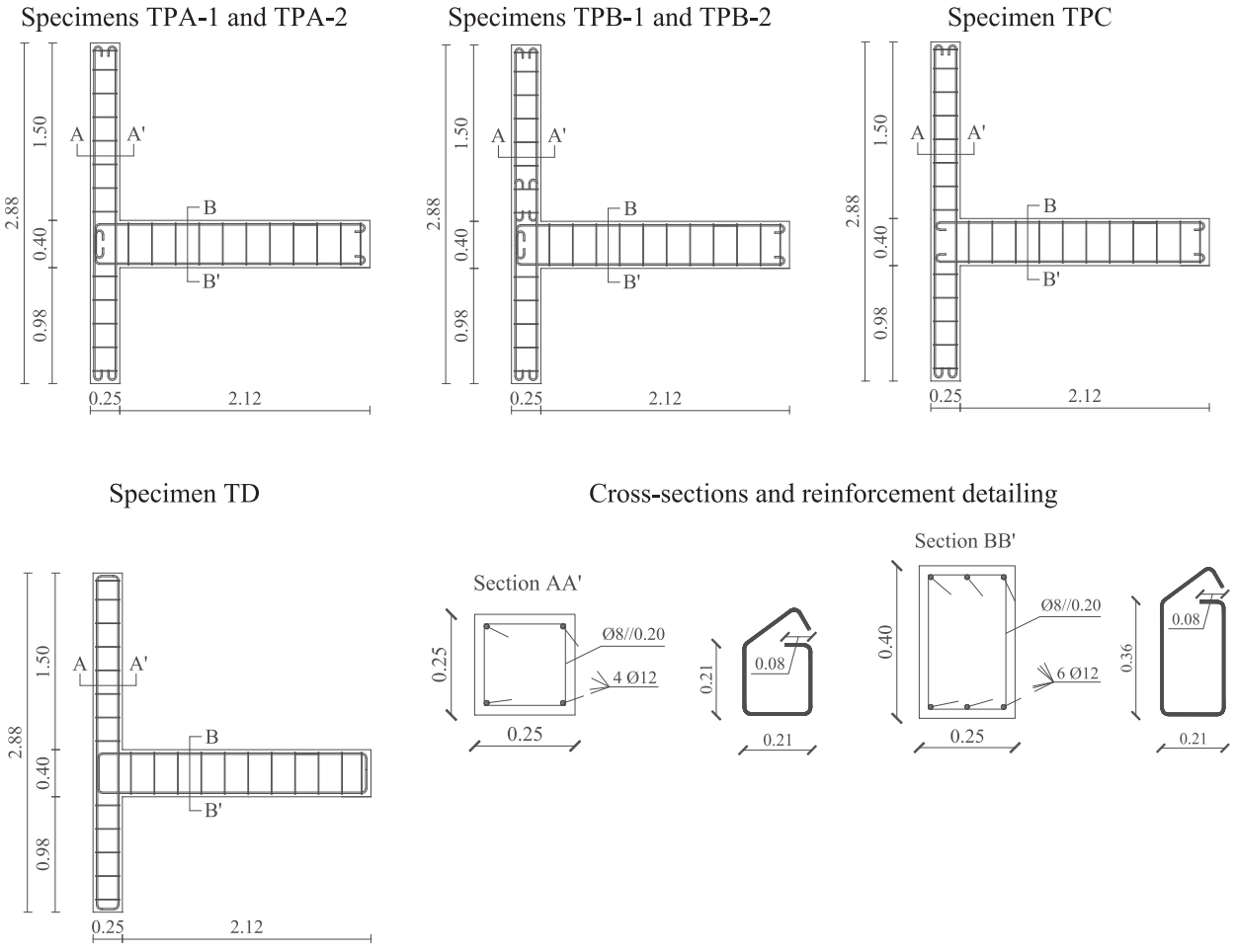

Fig. 1. Specimens (geometry, dimensions and reinforcement detailing).

specimens but built with deformed reinforcing bars.

Hot-rolled plain and deformed bars with grades A235 and A400NRSD were used as reinforcement of the specimens with plain and deformed bars, respectively. Concrete grade C16/20, according to EC-2 classification [27], was specified for the construction of the specimens. Steel reinforcing bars tensile tests were performed according to [28]. Table 1 summarises the mean properties of the concrete and steel used to build the specimens, where f_{cm} is the concrete compressive strength of cylinder samples (Ø15cmx30cm), f_{ctm} is the tensile strength of concrete, f_{ym} is the yield strength of reinforcement steel, f_{um} is the ultimate tensile strength of reinforcement and E_{ym} is the Young's modulus of the reinforcement.

2.2. Test setup, loading conditions and monitoring

Fig. 2 presents the loading conditions, lateral displacements history imposed, test-setup and monitoring scheme adopted in the tests. The specimens are tested in the horizontal position. The constant axial load (N) of 200kN (45 kip) is imposed in all tests by a hydraulic actuator placed at the top of the superior column associated to two tie rods linked to the base of the inferior column. To maintain the tie rods centred with the core joint during the test, two steel tubes are mounted at the base of the inferior column to extend the tie rods length. Therefore, the length of the tie rods in both sides of the joint (in the superior column and in the inferior column) is similar diminishing the second order effects at the columns' extremities. The monotonic tests (specimens TPA-1 and TPB-1) consist in apply an increasing displacement at the top of the superior column in the negative direction up to 6 % of drift. The cyclic tests are also carried out under displacement-controlled conditions of the imposed lateral displacements. The displacements' history imposed consists in three cycles applied for each of the following drift peak values (± %): 0.1, 0.2, 0.3 and then 0.5 to 3.5 with 0.5 increments (see Fig. 2a). The lateral displacements are imposed with a velocity rate ranging from 0.1 mm/second (0.0039 in/second) for the first cycles to 1.5 mm/second (0.059 in/second) for the last cycles.

The arrangement of the sensors used for monitoring is shown in Fig. 2d. Each pair of parallel displacement sensors located in each column or beam allows the computation of the axial deformation and the relative rotation, from which is calculated the mean curvature in the slice.

3. Experimental results and discussion

The experimental results are here presented and discussed, namely: hysteretic force-drift diagrams, force-drift envelopes, strength degradation, hysteretic dissipated energy evolution, equivalent damping-displacement ductility relationship, damages, drift components and joint shear strength. Comparisons of the response obtained for the specimens are made in order to show the response differences due to: i) reinforcing steel surface; ii) lapping of the longitudinal reinforcing steel bars; iii) anchorage of the beam longitudinal reinforcement in the joint. The damage patterns observed at the end of the tests are also compared.

3.1. Global force-drift response and strength degradation

The cyclic lateral force-drift response and the force-drift envelopes of the specimens tested are presented in Fig. 3 and Fig. 4, respectively. Each plot of Fig. 3 includes the response of two specimens aiming to highlight the differences for each variable under study, namely: bond properties (TPA-2 versus TD); lap-splice of the column longitudinal reinforcing bars (TPA-1 versus TPB-1 and TPA-2 versus TPB-2); and anchorage of the beam longitudinal reinforcing bars in the joint (TPA-2 versus TPC). In Fig. 4 is also compared the force-drift envelopes of the cyclic tests with the monotonic test results to show the difference between cyclic and monotonic loading (TPA-1 versus TPA-2 and TPB-1 versus TPB-2). Fig. 3 also shows the onset of each type of observed damage (the values are presented in Table 2), namely: cracking on beam (B. crack.), cracking on columns (C. crack.), cracking on the core joint (J. crack.), concrete cover spalling (C. spall.) and bar buckling.

Table 2 summarises the main values of the experimental response (for loading in positive direction) corresponding to: maximum force ($F_{c,max}$), drift at maximum force ($Drift_{Fc,max}$), ultimate force ($F_{c,ult}$), drift at ultimate force ($Drift_{Fc,ult}$) and drift for each type of observed damage. The ultimate force was defined according to Park and Ang [29], i.e. when was observed a 20 % strength reduction relatively to the maximum force.

Generically, the cyclic response obtained was symmetric and the maximum strength and initial stiffness (in the positive direction) are similar for all specimens once the material properties, cross-sections, load conditions and steel amount were similar in all specimens. However, considerable differences were observed on the response of the specimens in terms of damages, softening and strength degradation. The initial stiffness in the negative direction was around 20 % lower than in the positive direction for all specimens loaded cyclically. Generally, the cracking started at the beam for drift level of 0.2 % and then at the columns for drift level of 1.0 %, except in specimen TPA-1 that was 1.5 %. None shear cracks were observed in TPB specimens, but in the other specimens were observed shear cracks for drift levels ranging between 1.0 % (specimen TPC) and 2.5 % (specimen TPA-1). The cover spalling started for drift levels between 2.0 % (specimen TPC) and 5.5 % (specimen TPA-1). Bar buckling was observed in the core joint region for drift levels ranging from 2.0 % (specimen TPC) and 3.0 % (specimens TPA-2, TPB-2 and TD). In the monotonic tests was not observed bar buckling.

The differences in the hysteretic response of specimens TPA-2 and TD (Fig. 3a) were minor up to 2.5 % drift once the rupture of the specimens was mainly associated with the joint shear mechanism and not related

Table 1
Concrete and steel mechanical properties (mean values).

Specimen	Concrete		Steel						
			Bar surface	Ø8 mm			Ø12 mm		
	MPa (ksi)			MPa (ksi)		GPa (ksi)	MPa (ksi)		GPa (ksi)
	f_{cm}	f_{ctm}		f_{ym}	f_{um}	E_{ym}	f_{ym}	f_{um}	E_{ym}
TPA-1	24.5 (3.55)	2.3 (0.33)	Plain	410	495	198	405	470	199
TPA-2	25.8 (3.74)	2.5 (0.36)							
TPB-1	15.8 (2.29)	2.0 (0.29)		(59.5)	(71.8)	(28717)	(58.7)	(68.2)	(28863)
TPB-2	27.3 (3.95)	2.9 (0.42)							
TPC	23.8 (3.45)	2.6 (0.38)							
TD	21.5 (3.12)	2.4 (0.35)	Deformed	470	605	198	465	585	199
				(68.2)	(87.7)	(28717)	(67.4)	(84.8)	(28863)

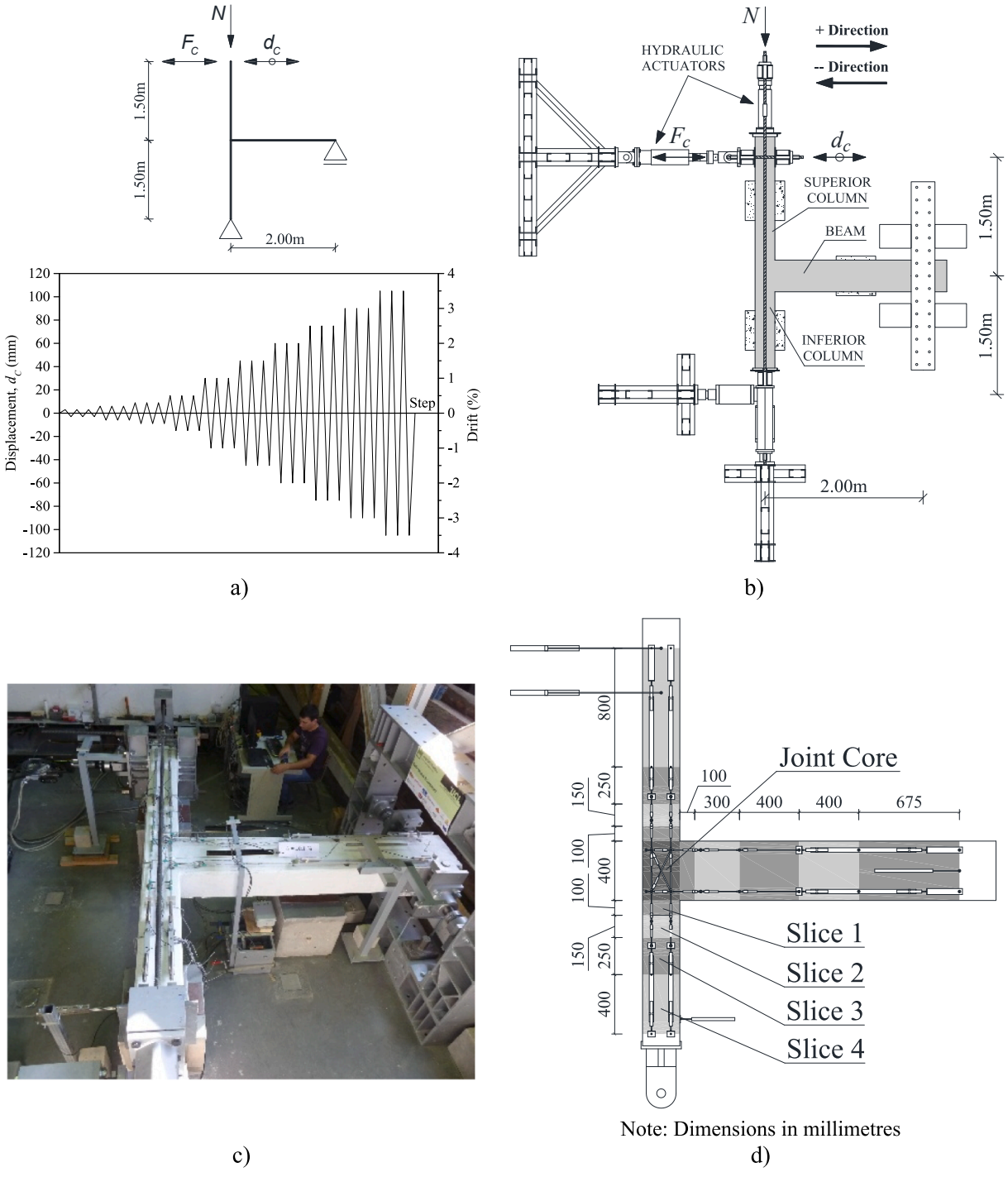

Fig. 2. Test-setup and monitoring: a) support and loading conditions idealized and imposed lateral displacement history; b) test setup schematics; c) general view; and d) monitoring scheme.

with the bond properties. Therefore, was not evident that the bond properties have influenced the global cyclic response of the exterior beam-column joint with plain reinforcing bars. The lap-splice in the superior column of specimen TPB-2 did practically not influence the hysteretic response when compared to specimen TPA-2, as well. However, the hysteretic response of specimen TPC showed larger softening and strength degradation than in the reference specimen. Moreover, specimen TPC achieved the ultimate force for a drift demand of 1.4 % while for the reference specimen was 2.6 %. The weak anchorage of the beam longitudinal bars in the joint of specimen TPC lead to larger strength degradation and softening and the ultimate force was reach for drift level that was almost half of the one for specimens with a proper anchorage detailing (TPA-2 and TPB-2). The specimens monotonically loaded showed similar behaviour up to 2.0 % drift and then was observed softening in specimen TPA-1 and a plateau in specimen TPB-1. Therefore, specimen TPA-1 reach the ultimate force for 4.3 % drift and specimen TPB-1 did not achieve the ultimate force up to 6.0 % drift. The response of specimens tested monotonically match with the force-drift envelopes of the corresponding specimens tested under cyclic loading up to achieve the maximum strength.

The strength degradation (SD) evolution (from 0.3 % drift) between the first and second and between the first and third cycles of each drift

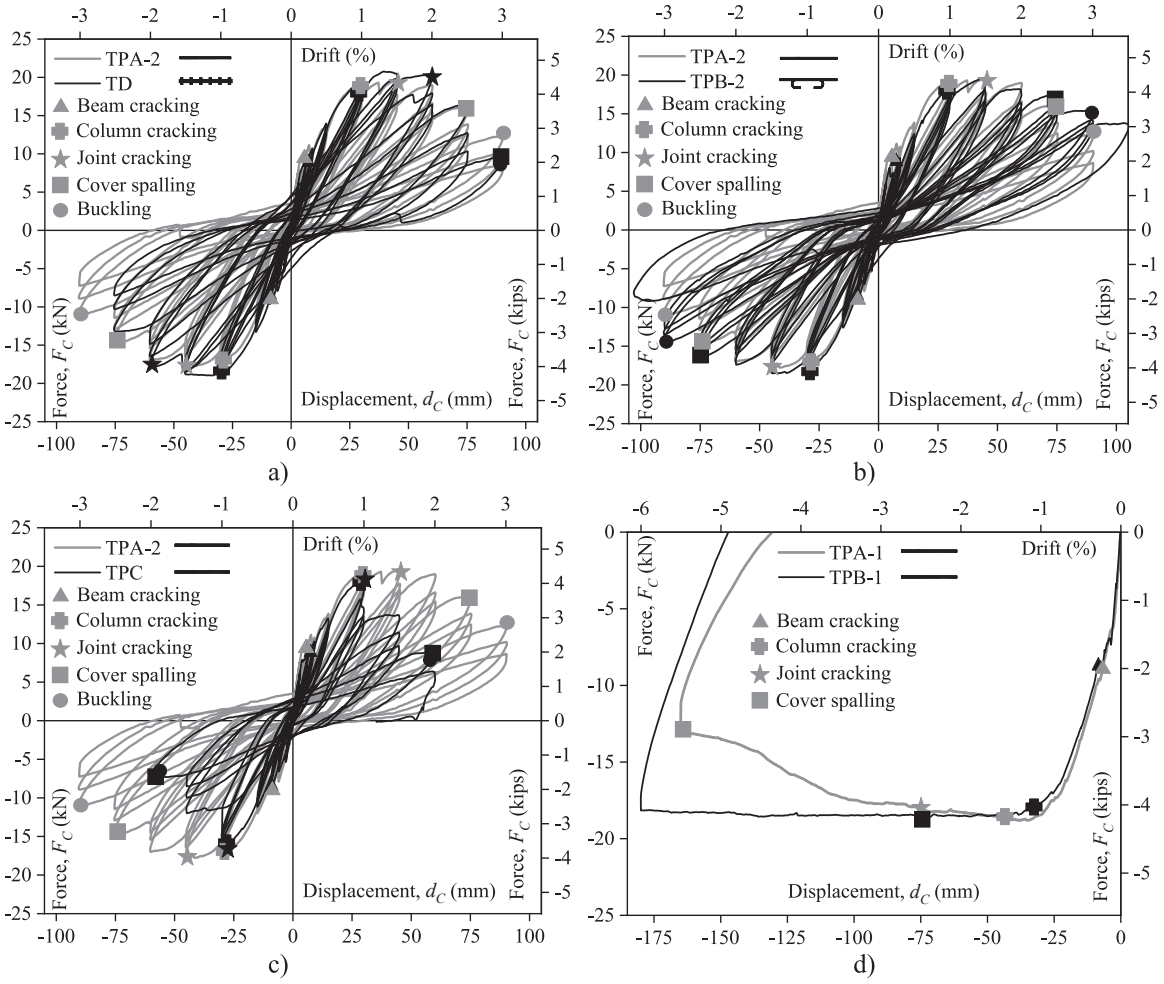

Fig. 3. Lateral force-drift relationships: a) TPA-2 versus TD; b) TPA-2 versus TPB-2; c) TPA-2 versus TPC; and d) TPA-1 versus TPB-1. (Note: 1 mm = 0.0394 in).

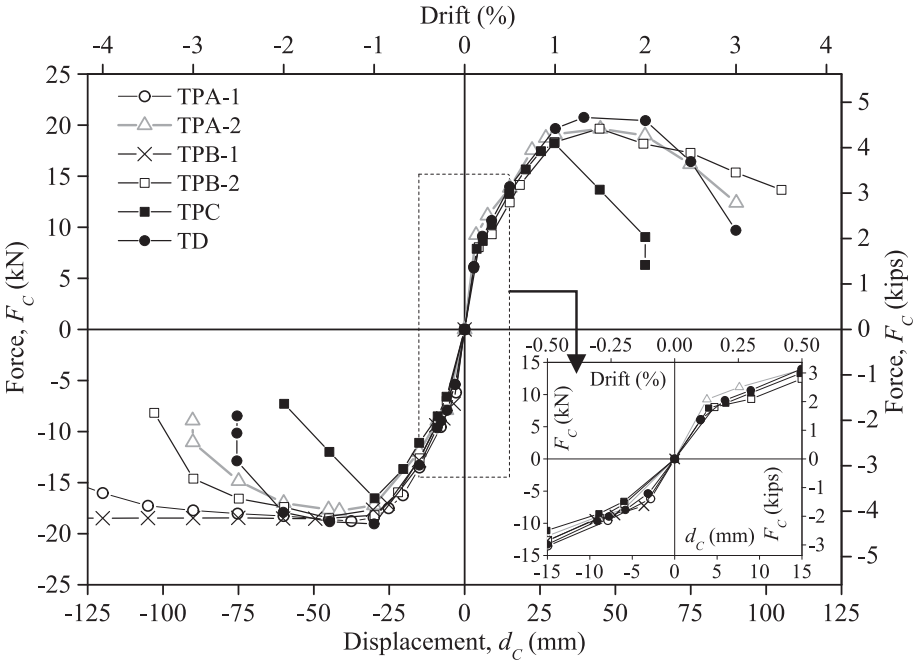

Fig. 4. Experimental force-drift envelopes. (Note: 1 mm = 0.0394 in).

Table 2
Force and drift for the maximum strength, ultimate points and observed damages.

#	$F_{c,max}$ kN (kip)	$Drift_{Fc,max}$ %	$F_{c,ult}$ kN (kip)	$Drift_{Fc,ult}$ %	Observed damages - *Drift (%)*				
					B. crack.	*C. crack*	*J. crack*	*C. Spall.*	*Buckling*
TPA-1	18.8 (4.23)	1.3	15.0 (3.37)	4.3	0.2	1.5	2.5	5.5	–
TPA-2	19.6 (4.41)	1.5	15.7 (3.53)	2.6	0.2	1.0	1.5	2.5	3.0
TPB-1	18.5 (4.16)	1.7	–	–	0.2	1.0	–	–	–
TPB-2	19.7 (4.43)	1.5	15.8 (3.55)	2.9	0.2	1.0	–	2.5	3.0
TPC	18.2 (4.09)	1.0	14.6 (3.28)	1.4	0.2	1.0	1.0	2.0	2.0
TD	20.8 (4.68)	1.3	16.6 (3.73)	2.5	0.2	1.0	2.0	3.0	3.0

level is shown in Fig. 5. In this figure is also present the best linear fitting curves and corresponding equations. In the equations the strength degradation and drift levels are expressed in percentage. For specimens TPA-2, TPB-2 and TD the strength degradation between the second and third cycles corresponds to 55 % of the strength degradation between the first and second cycles. For specimen TPC this percentage is 74 %. The fitted curves of specimens TPC and TD have the largest slopes, therefore the strength degradation for high drift levels was larger than in the reference specimen (CPA-2).

3.2. Dissipated energy evolution

The hysteretic dissipated energy is a parameter that evaluate the capacity of the element to dissipate energy under cyclic loading. The hysteretic dissipated energy evolutions, calculated as the area under the experimental lateral force–displacement diagrams, are shown in Fig. 6.

The dissipated energy evolutions were similar for all specimens up to 1.5 % drift, i.e. until reach the maximum strength. Then specimen TD had dissipated more energy than the other specimens due probably to the better bond properties. At the end of the third cycle of 2.5 % drift demand imposed, specimen TD dissipated more 21 % and 43 % than the reference specimen (TPA-2) and specimen TPB-2, respectively. Similar conclusions were observed by other authors for interior beam-column joints [8] and columns [30]. Specimen TPC had dissipated less 18 % energy than the reference specimen at the end of the third cycle of 2.0 % drift, being the specimen with lower capacity to dissipate energy. Specimen TPB-2 dissipated less 13 % energy than specimen TPA-2 for 3.0 % drift showing that the lap-splice of the longitudinal bars in the superior column may reduce the energy dissipation capacity.

The dissipated energy was also quantified by components (joint, beam and columns) for each drift demand level. Therefore, the results evidence the contribution of each component for the total energy. The dissipated energy is commonly associated with the damage in the RC elements, thereby elements with larger damage usually dissipate more energy than elements with lower damage level. The results here present

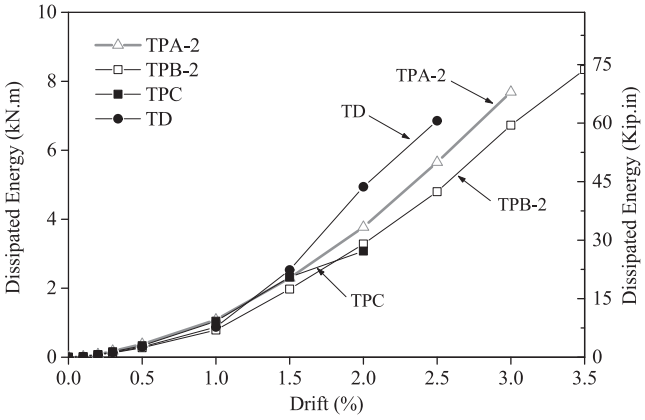

Fig. 6. Evolutions of the hysteretic dissipated energy.

are aligned with the damages observed during the cyclic tests.

The dissipated energy at the joint was computed as the area under the lateral shear force versus joint distortion diagram. The horizontal shear force in the joint (V_{jh}) was calculated by Equation (1), where M_b is the beam moment at the face of the joint core, j_d is the lever arm between the tensile forces and the centroid of the compressive force at the joint-beam interface (in this study the average value of j_d is 0.90·d, where d is the effective depth), and V'_c is the shear force in the base of the superior column.

$$V_{jh} = \frac{M_b}{j_d} - V'_c \tag{1}$$

The dissipated energy at the beam and columns was computed integrating along the elements length the experimental moment–curvature results and assuming a linear distribution of the curvatures from the elements' extremity to the interface between slice 1 and slice 2 (see Fig. 2d) and assuming a constant distribution of

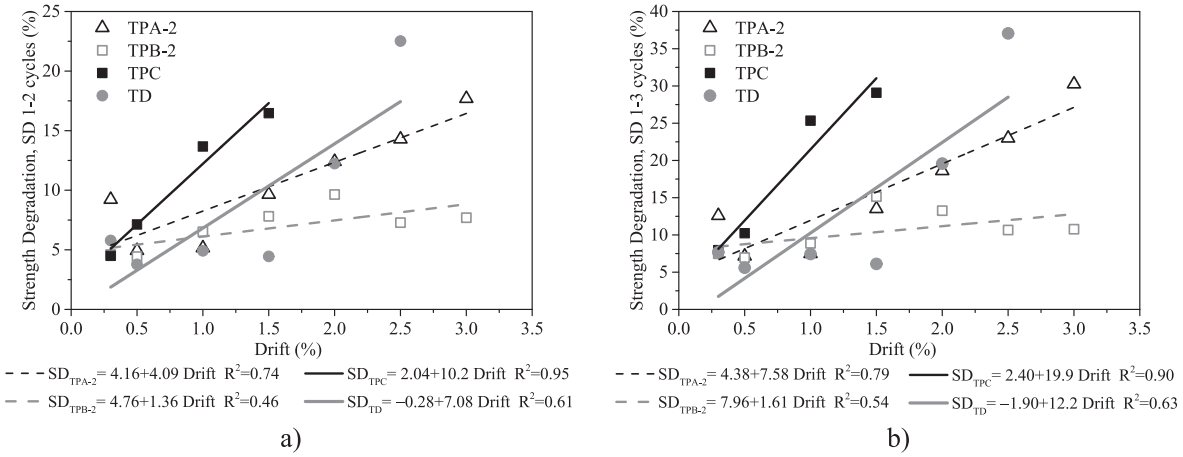

Fig. 5. Strength degradation: a) between the first and second cycles; and b) between the first and third cycles.

curvatures in slice 1.

The total dissipated energy calculated as the sum of the dissipated energy of the joint, beam and columns for each drift demand was compared with the corresponding experimental total energy dissipation (Fig. 6). For drift levels between 0.2 % and 3.5 %, the sum of the dissipated energy computed independently (joint, beam and columns) represents in average 94 % of the total experimental dissipated energy (coefficient of variance equals to 16 %). Thus, the methodology adopted to compute the dissipated energy at the components give a good estimative of the fraction of dissipated energy per component.

The evolutions of the dissipated energy contribution of the joint, beam and columns to the total dissipated energy are represented in Fig. 7. The dissipate energy showed in Fig. 6 is similar up to 1.5 % drift for all specimens. However, looking for each component (Fig. 7) it had considerable differences between the specimens.

At the end of the tests, the dissipated energy at the columns represented a percentage ranging from 10 % (TPC) to 45 % (TPB-2) of the total energy. The percentage at the beam varies between 45 % (TPC) and 60 % (TD). In global terms, the beam is the component that dissipated more energy when compared with joint and columns.

3.3. Displacement ductility and equivalent damping

The equivalent damping is commonly used to calibrate numerical macro-elements that represent the global behaviour of structural elements such as columns, beam-column joints and beams. The equivalent damping was calculated according to the methodology present in Varum [2]. Equation (2) was used to compute the equivalent damping (ξ_{eq}), where $A_{half\text{-}loop}$ is the area within "half" force–displacement cycle and F_{max} and D_{max} are the maximum force and maximum displacement achieved in the respective half cycle.

$$\xi_{eq} = \frac{1}{\pi}\cdot\frac{A_{half-loop}}{F_{max}} \quad (2)$$

The equivalent damping is presented in this work as a function of the displacement ductility. The displacement ductility was defined as the ratio between the maximum imposed displacement in each cycle and the yield displacement (Δ_y) that was calculated according to Annex B.3 of EC8-1 [31] and present in [30].

Table 3 resumes the yield force ($F_{c,y}$), the drift at yield ($Drift_y$), the displacement ductility at the ultimate force ($\mu_{\Delta,ult}$), of the fitted bi-linear curves. Table 3 also presents the equivalent damping value at the ultimate force ($\xi_{eq,ult}$) obtained from the best-fit curves (see Fig. 8).

The yield drift was similar for all specimens, except for specimen TPB-1 (see Table 3). However, the displacement ductility at ultimate force was almost half in specimen TPC than in the other specimens cyclically tested. The displacement ductility values at the ultimate force were in average 37 % lower than the corresponding values obtained for interior beam-column joints built with plain reinforcing bars and tested in the same test setup [32]. This notable difference was related with the

Table 3
Yield force, yield drift, displacement ductility and equivalent damping at ultimate force.

Specimen	$F_{c,y}$ kN (kip)	$Drift_y$ %	$\mu_{\Delta,ult}$	$\xi_{eq,ult}$ %
TPA-1	17.7 (3.98)	0.58	7.47	–
TPA-2	17.6 (3.96)	0.59	4.30	9.96
TPB-1	18.3 (4.11)	0.66	–	–
TPB-2	17.4 (3.91)	0.60	4.86	9.49
TPC	16.0 (3.60)	0.58	2.40	12.57
TD	18.7 (4.20)	0.60	4.17	11.85

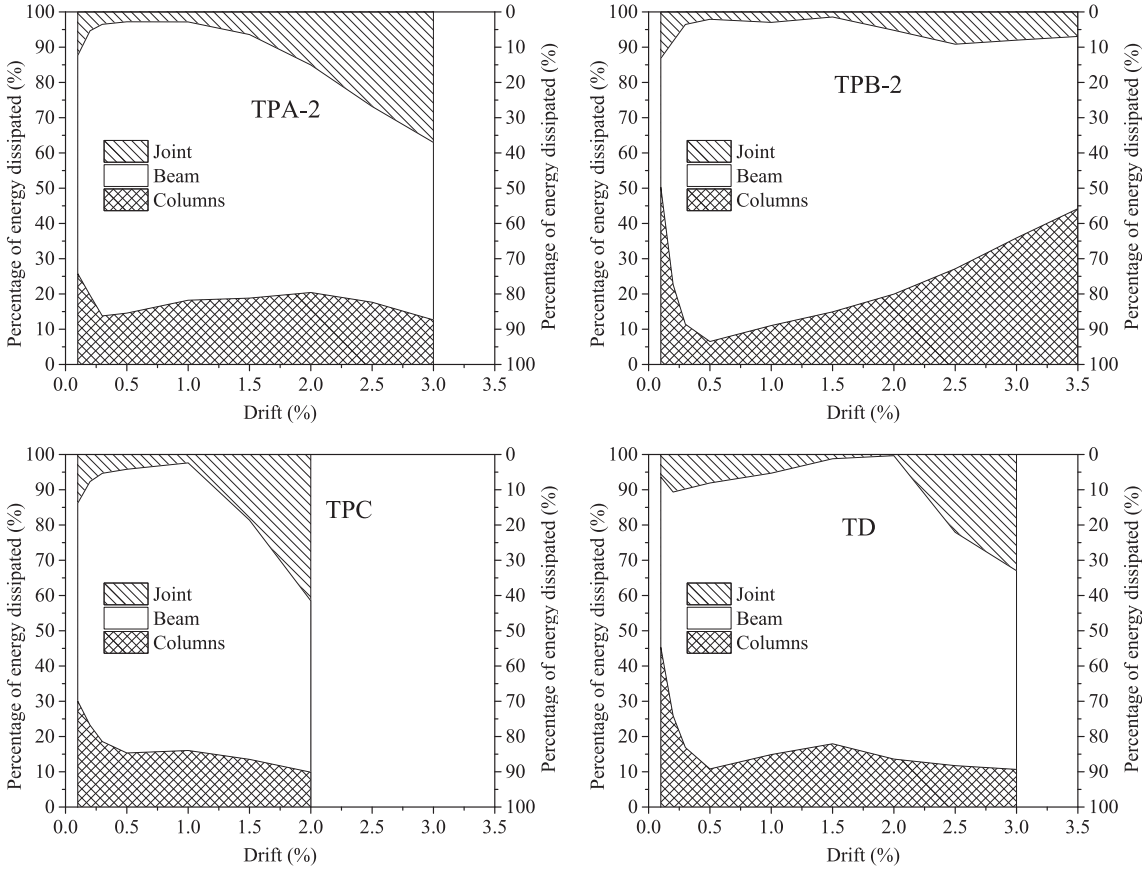

Fig. 7. Contribution to the total dissipated energy of different components: joint, beams and columns.

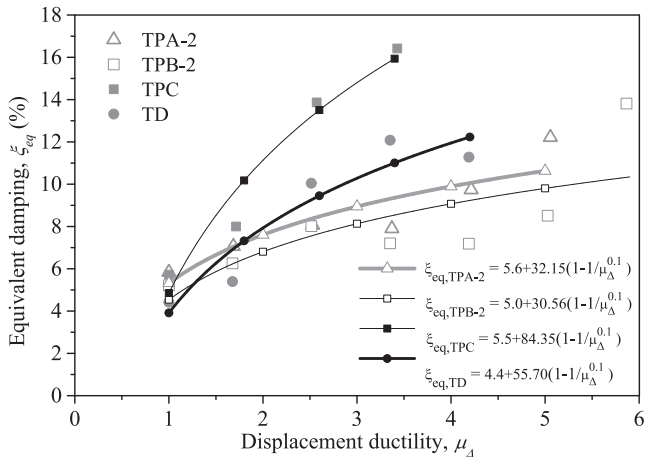

Fig. 8. Equivalent damping-displacement ductility diagrams.

weaker concrete confinement and with the beam anchorage of the longitudinal reinforcing bars in the core of the exterior joints. Specimen TPC was the one with larger equivalent damping at ultimate force because of the simple anchorage of the beam longitudinal reinforcing bars. Specimen TD also had considerable larger (19 % more) equivalent damping at ultimate force than the reference specimen.

The equivalent damping obtained from the experimental results, as function of the displacement ductility (μ_Δ) and the corresponding best-fit curves defined according to the general expression proposed by Priestley [33] (see Table 4) is presented in Fig. 8. In specimen TPC, the increase of the equivalent damping with the displacement demands was more evident due to the early damage observed in the joint. In specimen TD the damping increases more with the displacement ductility than in the reference specimen as observed in other studies [8,32] performed on interior RC beam-column joints built with plain reinforcing bars.

Table 4 presents the general equivalent damping-displacement ductility equation proposed by Priestley [33] (Equation 3), the expression proposed by Melo et al. [30] (Equation 4) based on the experimental results of columns, the expression proposed by Melo et al. [32] based on experimental results of interior beam-column joints and other three curves (Equations (6) to (8)) which were fitted to the experimental results here presented and fitted to experimental results of other authors [2,8]. Equations (4) to (8) are referenced to RC elements built with plain reinforcing bars. Equations (4) to (8) follow the generic form of Equation (3), considering $\beta = 0.1$ and adopting for a parameter and for the initial damping (ξ_0) the values resulting from the best-fit to the respective experimental results.

Table 4
Equivalent damping-displacement ductility relationships.

Experimental data source	Element type	Equation		Equation proposed in the literature
	Generic	$\xi_{eq} = \xi_0 + a\cdot\left(1-\frac{1}{\mu^\beta}\right)$	(3)	Priestley [33]
	Columns	$\xi_{eq} = 3.8 + \frac{146}{\pi}\left(1-\frac{1}{\mu^{0.1}}\right)$	(4)	Melo et al. [30]
	Interior beam-column joints	$\xi_{eq} = 5.9 + \frac{68}{\pi}\left(1-\frac{1}{\mu^{0.1}}\right)$	(5)	Melo et al. [32]
Fernandes et al. [8]		$\xi_{eq} = 4.8 + \frac{67}{\pi}\left(1-\frac{1}{\mu^{0.1}}\right)$	(6)	
	Exterior beam-column joints	$\xi_{eq} = 11.2 + \frac{114}{\pi}\left(1-\frac{1}{\mu^{0.1}}\right)$	(7)	Risi and Verderame [14]
Presented experimental data		$\xi_{eq} = 5.2 + \frac{134}{\pi}\left(1-\frac{1}{\mu^{0.1}}\right)$	(8)	

Fig. 9 compares the experimental results reported in this work with and the curves given by Equations (4) to (7). In the same figure is represented the fitted curve to the experimental results here reported (Equation 8). The best-fit curve given by Equation (8) match better with the curve obtained from experimental results of structures governed by column failure mechanisms (Equation (4)), than the curves obtained from experimental results of interior beam-column joints (Equation (5)). The curve (Equation (7)) presented by Risi and Verderame. [14] for exterior beam-column joints with plain reinforcing bars has similar evolution tends than the obtained experimental best-fit curve but with higher initial equivalent damping.

3.4. Observed damages

The observed cracks for drift levels of 0,3%, 0,5%, 1,0% and 2,0% are presented in Table 5. The crack pattern observed (face with monitoring) at the end of the experimental tests is shown in Fig. 10. For the cyclic tests two different failure modes were observed: i) shear failure of the core joint followed by concrete spalling and buckling of the exterior longitudinal reinforcing bars of the columns in the core joint (specimens TPA-2, TPC and TD); and ii) concrete spalling followed by buckling of the exterior longitudinal reinforcing bars of the columns in the core joint (specimen TPB-2). Buckling occurred due to the poor confinement in the joint because of no transverse reinforcement in this zone. Most of the flexure cracks were on the stirrups area due to the concrete discontinuity caused by the stirrups.

In specimen TPC a large concrete spalling area (concrete wedge mechanism) was observed in the core joint due to the tension forces that the anchorage hook of the longitudinal rebars of the beam induce in the concrete and also due to buckling of the external longitudinal rebars of columns in the core joint. In specimen TD, the concrete damage was more distributed along the beam' span than in the other specimens built with plain reinforcing bars, that is in agreement with observations made by other authors [8,30,32] as a consequence of the better bond conditions provided by deformed bars. The dissipated energy of each component presented in Fig. 7 and the corresponding damage are correlated. Despite of the observed damage on the columns (see Fig. 10) looks minor, there are big cracks in the column-joint interface that justify the dissipated energy showed in Fig. 7.

3.5. Displacement components

Several deformation mechanisms contribute to the lateral displacement (d_c) when it is imposed at the top of the superior column, namely: i) shear in columns; ii) bending in columns and beam; iii) joint relative rotation; and iv) joint shear distortion. The lateral displacement at the top of the specimen was assumed as the sum of the different deformation mechanisms above mentioned.

Elastic shear modulus (G) of 7.25GPa (1052ksi) and constant shear distribution along the column's length were considered to compute the lateral displacement due to shear. The elastic shear modulus was calculated considering the Young's modulus of the concrete (estimated from the average concrete compressive strength) and considering a Poisson's ratio of 0.2.

The lateral displacement due to bending in columns and beam was divided in two components: a) linear elastic; and b) non-linear bending. The lateral displacement of each bending component was calculated according to the methodology present in [32] for interior beam-column joints built with plain reinforcing bars.

The "joint relative rotation" component represents the lateral displacement caused by the deformations in the core joint apart from the joint shear distortion, i.e. the contribution of the joint expansion and the relative rotation between the top and bottom joint sections. The lateral

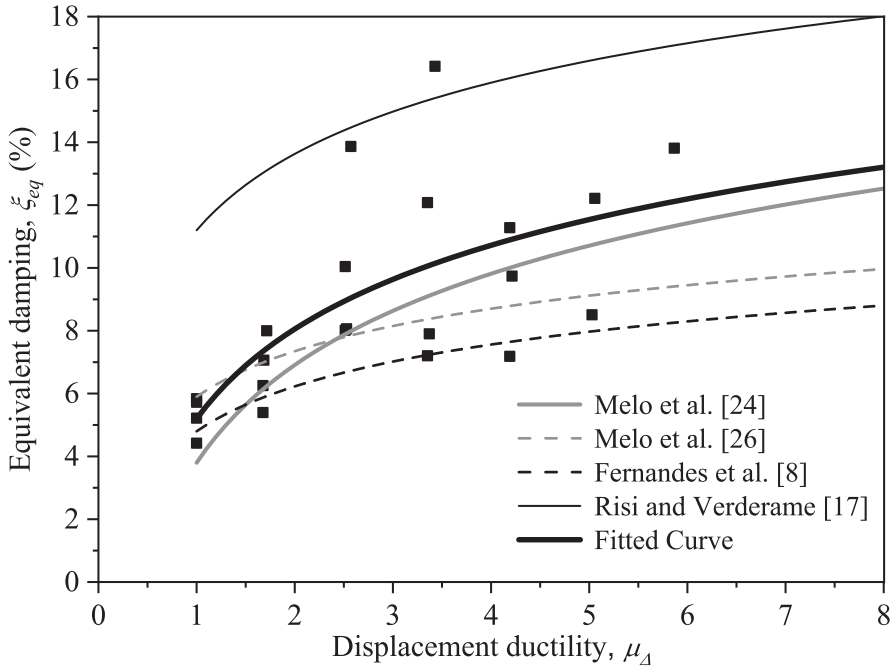

Fig. 9. Equivalent damping-displacement ductility diagrams: comparison between all experimental results and curves fitted to experimental results of other authors for elements with plain reinforcing bars [8,14,30,32].

displacement of this component was calculated using the relative displacements measured by the diagonal potentiometers in the core joint to compute the relative joint rotation and then it was multiplied by the length of the column.

The displacement component due to joint shear distortion was determined based on the deformations measured by the potentiometers placed diagonally on the core joint and according to the methodology present in [34].

In general terms, a good agreement was found between the experimental displacement (d_c) and the sum of each displacement component (above explained), which permits conclude that the methodology used allows the identification of the deformation mechanism and their influence in the response of specimen. For drift values ranging from 0.3 % to 3.0 % the average difference observed between the analytical and the experimental results was 16 % with a coefficient of variance equals to 0.11.

The contribution for the lateral displacement of the different deformation mechanisms: columns shear, linear elastic bending in columns and beam, non-linear bending in columns and beam, joint relative rotation and joint shear distortion, for drift demands ranging from 0.2 % to the drift of the end of each test, is shown in Fig. 11. For small drift demands (up to 0.2 %) the relative displacements measured in some potentiometers are close to their sensibility and thereby these results were excluded for this analysis.

The relative contribution of the shear deformation in columns to the lateral displacement was small for all specimens, signifying around 2.0 % of the lateral displacement for 0.2 % drift demand and 0.2 % for 3.0 % drift. These results are in accordance with observations made in similar tests carried out on interior beam-column joints [32].

For all specimens, the relative contribution of the elastic bending in columns and beam to the lateral displacement always decreased with the increased of the drift demands. For drift demands of 0.2 % the elastic bending contribution represented between 70 % (TPB-2) and 85 % (TPA-2) of the total lateral displacement and then decreased almost linearly (except in specimens TPA-1 and TPB-1 where it decreased with a parabolic shape) until the end of the tests where it represented between 9 % and 13 % of the total displacement.

The relative contribution of the non-linear bending in columns and beam had different evolutions for each specimen. The specimens monotonically tested showed larger contribution of the non-linear bending, because of larger width bending cracks in the beams, than in the corresponding specimens cyclically tested.

The contribution of the joint relative rotation to the total lateral displacement increased with the damages in the core joint for drift demands larger than 1.0 % for specimen TPC and 1.5 % for the other specimens (onset of the shear cracks in the core joint) and may represents up to 70 % (TPC) of the total displacement at the end of the test.

The contribution of the joint shear distortion to the lateral displacement also increased with the damage level in the core joint being almost zero at 0.2 % drift and varying between 0.2 % and 13 % at the end of the tests.

Comparing the relative contributions to lateral displacement of the different deformation mechanisms of all specimens, there are evident differences between the results of the monotonic tests and the cyclic tests and between the results of specimens TPB-2, TPC and TD when compared with the reference specimen.

4. Joint shear strength

The shear stress in the core joint is commonly expressed as nominal shear stress or as principal compression/tensile stresses. The horizontal shear stress (ν_{jh}) in the core joint can be calculated by Equation (9) [35], where V_{jh} is the horizontal shear force in the joint, calculated by Equation (1); b_c is the columns width; and h_c is the depth of the columns. Based on the Mohr's circle, the principal tensile stresses (p_t) at the mid-depth of the core joint is given by Equation (10) [36], where f_a is the nominal axial compressive stress on the column calculated by Equation (11), and compressive stresses are taken as negative.

$$\nu_{jh} = \frac{V_{jh}}{b_c \cdot h_c} \tag{9}$$

$$p_t = \frac{-f_a}{2} + \sqrt{\left(\frac{f_a}{2}\right)^2 + \nu_{jh}^2} \tag{10}$$

Table 5
Observed damage at drift levels of 0,3%, 0,5%, 1,0% and 2,0%.

Specimen	Drift 0,3%	0,5%	1,0%	2,0%
TPA-1	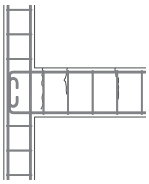	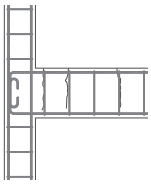	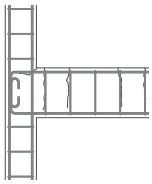	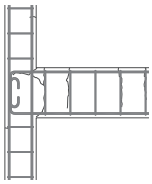
TPA-2	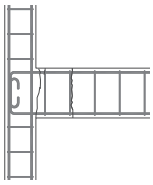	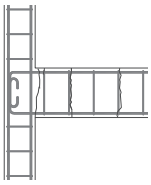	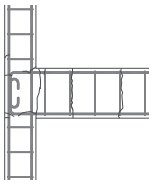	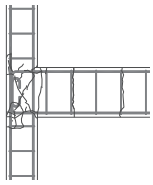
TPB-1	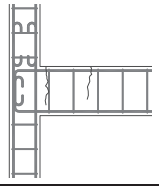	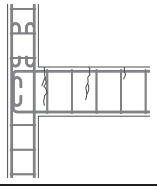	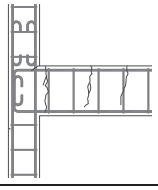	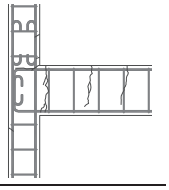
TPB-2	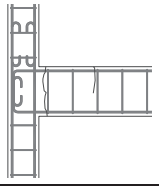	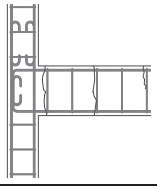	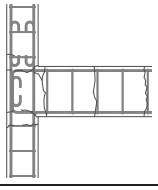	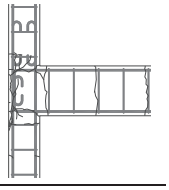
TPC	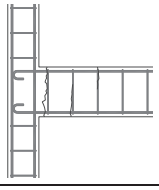	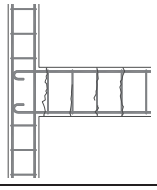	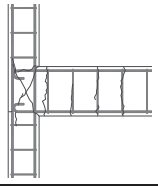	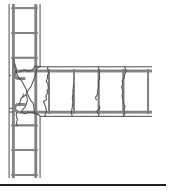
TD	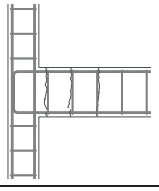	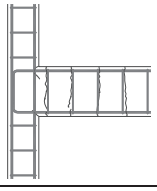	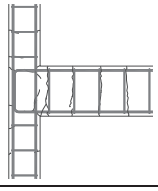	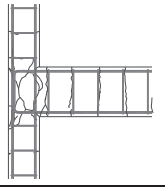

$$f_a = \frac{N}{b_c \cdot h_c} \tag{11}$$

Tsonos [35] proposed a formulation to predict the beam-column joint ultimate shear strength based on the strut-and-tie mechanism. This model assumes biaxial concrete strength curve as a fifth-degree polynomial and solve this fifth-order polynomial equation. The normalized joint shear strength (γ) is determined by solving Equation (12), where α is the joint aspect ratio (beam depth / column depth) and f_c is the concrete compressive strength. An iterative process is needed to solve Equation (12) and obtain the value of γ. The joint shear strength $\overline{V}_{jh}^{Tsonos}$ is given by $\gamma \bullet \sqrt{f_c}$.

$$\left[\frac{\alpha\gamma}{2\sqrt{f_c}}\left(1+\sqrt{1+\frac{4}{\alpha^2}}\right)\right]^5 + \frac{5\alpha\gamma}{\sqrt{f_c}}\left(\sqrt{1+\frac{4}{\alpha^2}}-1\right) = 1 \tag{12}$$

Hwang and Lee [37] developed a joint strength model to satisfy equilibrium, compatibility and constitutive laws of cracked reinforced concrete. This model assumes that the joint shear resisting mechanisms are composed of three mechanisms: i) diagonal strut mechanism; ii) horizontal mechanism; and iii) vertical mechanism. The shear strength of the joint is defined when the compressive stress and strain of the concrete diagonal strut reach a limit calculated in the calculating process. The stress and strain values are dependent on each other and an iterative procedure is needed to compute the joint shear strength. In this work the joint shear strength computed according to the Hwang and Lee model followed the flow chart present in Fig. 9 of [37].

According to Eurocode 8–3 (EC8-3) [38] in the assessment of existing RC structures, the shear demand and shear capacity on the joints, for limit state of near collapse, is evaluated in accordance with Eurocode 8-1 (EC8-1) [31]. According to EC8-1 the diagonal compression induced in the joint by the diagonal strut mechanism shall not exceed the compressive strength of the concrete (f_c) in the presence of transverse tensile strains. For exterior joints, this requirement may be satisfied if Equation (13) is fulfilled, i.e. if the horizontal shear force in the joint does not exceed $\overline{V}_{jh}^{EC8}$. In Equation (13), ν is the normalized axial load in the column above the joint, h_{jc} is the distance between extreme layers of column reinforcement and η is given by Equation (14), where f_{ck} is the

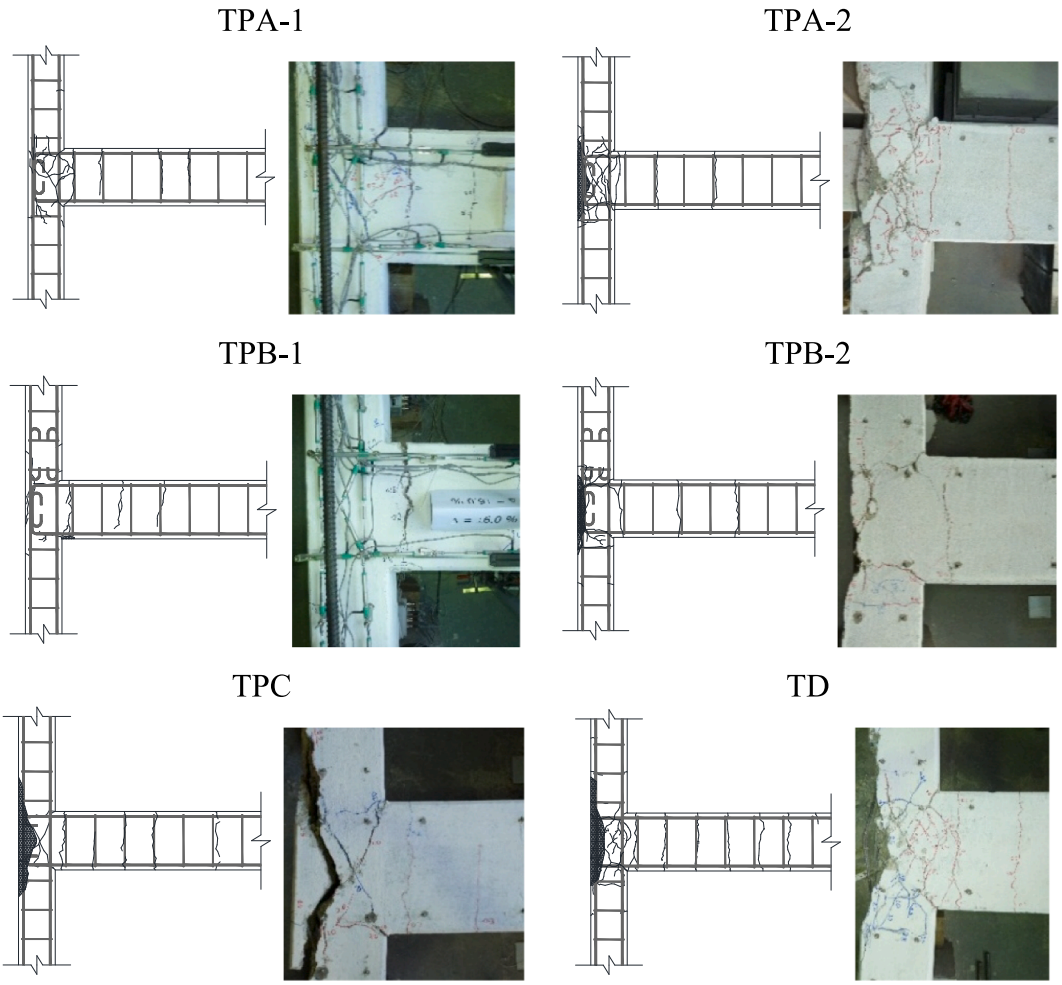

Fig. 10. Final damage state for the top face of the specimens.

characteristic compressive concrete strength in MPa.

$$V_{jh} \leq 0.8 \cdot \eta \cdot fc \cdot \sqrt{1 - \frac{\nu}{\eta}} \cdot b_j \cdot h_{jc} = \overline{V}_{jh}^{EC8} \tag{13}$$

$$\eta = 0.6 \cdot (1 - f_{ck}/250) \tag{14}$$

ACI 369.1M-17 [39] specify that the joint shear strength $\overline{V}_{jh}^{ACI369}$ shall be calculated using the general procedures of *ACI* 318-19 [40] and calculated according to equation (15), where λ is 1.0 for normal weight aggregate concrete; γ is 6 for exterior joints without transverse beams and with nonconforming transverse reinforcement; f_{ck} is the characteristic concrete cylinder compressive strength in MPa; and, A_j is the effective horizontal joint area that for the specimens under study corresponds to the column cross-section area.

$$\overline{V}_{jh}^{ACI369} = 0.083 \bullet \lambda \bullet \gamma \bullet \sqrt{f_{ck}} \bullet A_j \tag{15}$$

Table 6 presents the maximum experimental horizontal shear force in the joint ($V_{jh,\max}$), the corresponding drift ($\Delta_{Vjh,\max}$), the values of the normalized joint shear strength obtained according to Tsonos model (γ^{Tsonos}) and the maximum compressive stress computed according to Hwang and Lee model $\sigma_{d,max}^{Hwang\&Lee}$. Moreover, it also presents the ratios between the maximum horizontal shear force in the joint and the: Tsonos [35] prediction ($\overline{V}_{jh}^{Tsonos}$); Hwang and Lee [37] prediction ($\overline{V}_{jh}^{Hwang\&Lee}$); EC8-1 [31] limit ($\overline{V}_{jh}^{EC8}$); and *ACI* 369.1M-17 [39] limit ($\overline{V}_{jh}^{ACI369}$). The maximum shear capacity predicted by both models as well as the EC8 limit are significantly larger than the experimental maximum horizontal shear force. Considering that in all specimens (except in specimens TPB) were observed shear cracks in the core joint, the models and the EC8 overestimate the shear capacity of the joints. The standard *ACI* 369.1M-17 [39] was developed for seismic evaluation of existing RC structures. This justifies the good shear capacity prediction obtained by *ACI* 369.1M-17. Table 6 also presents the mean values of the ratios between the experimental maximum shear force of the specimens with plain bars and the predicted values by the models and codes show that the best prediction was given by the standard *ACI* 369.1M-17, followed by Hwang and Lee model, EC8-1 limit and Tsonos prediction.

For specimen TPB-1 the predictions were better than for the other specimens once that this specimen had lower compressive concrete strength than the other specimens and it is an important input in the considered models. For specimen TD the models and codes also overestimate the maximum shear capacity, but the difference between the experimental value and the analytical values was lower.

The envelopes of the principal tensile stress (normalized by $\sqrt{f_c}$) – drift relationship is displayed in Fig. 12. Based on the test observations, joint cracking starts when the maximum principal tensile stress (p_t) was achieved. The asymmetry of the plot present in Fig. 7 was related to the difference of the axial load between the superior and inferior columns due to the beam reaction. For drift demands in the positive direction the axial load was lower in the inferior column than in superior column, but for the negative direction it reverses. For 1.5 % drift the difference of the axial load in the inferior column between the positive and negative directions may represents 17 % of the axial load imposed at the top of the superior column. The observed maximum principal tensile stresses were around three times lower than the ones present in Chalioris et al. 2008

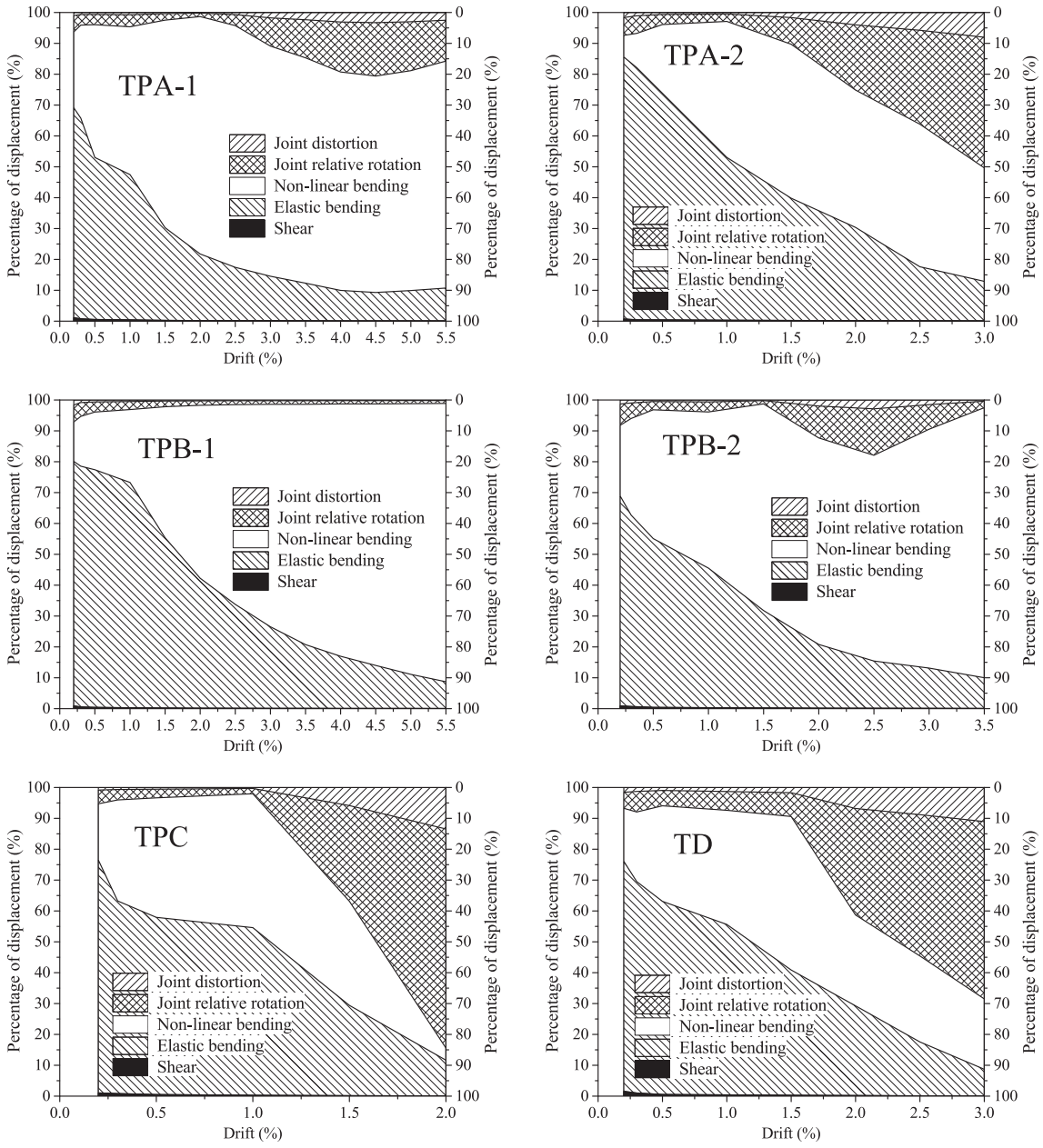

Fig. 11. Contribution to the total lateral displacement of the different deformation mechanisms: columns shear, linear elastic bending in columns and beam, non-linear bending in columns and beam, joint relative rotation and joint shear distortion.

Table 6
Maximum shear force ratios.

Specimen	$\Delta_{Vjh,\max}$ %	$V_{jh,\max}$ kN	γ^{Tsonos}	$\sigma_{d,max}^{Hwang\&Lee}$ MPa	$\frac{V_{jh,max}}{V_{jh}^{Tsonos}}$	$\frac{V_{jh,max}}{V_{jh}^{Hwang\&Lee}}$	$\frac{V_{jh,max}}{V_{jh}^{EC8}}$	$\frac{V_{jh,max}}{V_{jh}^{ACI369}}$
TPA-1	−1.2	−131.7	1.02	16.3	0.42	0.75	0.45	1.04
TPA-2	1.5	137.5	1.05	17.1	0.41	0.76	0.43	1.05
TPB-1	−2.4	−130.3	0.84	10.6	0.59	0.97	0.81	1.34
TPB-2	1.5	137.7	1.08	18.1	0.39	0.73	0.40	1.01
TPC	1.0	126.6	1.01	15.8	0.41	0.74	0.46	1.03
Mean value					0.44	0.79	0.51	1.09
CoV					0.18	0.13	0.34	0.13
TD	1.3	145.4	0.95	14.3	0.62	0.90	0.62	0.50

[41] for exterior beam-column joints with X-bars in the core joint. Generically, the principal normalized tensile stress was similar for specimens TPA-2, TPB-2 and TPC up to reach the maximum stress and it increased linearly. The maximum principal normalized tensile stress observed in specimen TD was in average 27 % larger than obtained in specimen TPA-2. Also, the maximum principal normalized tensile stress

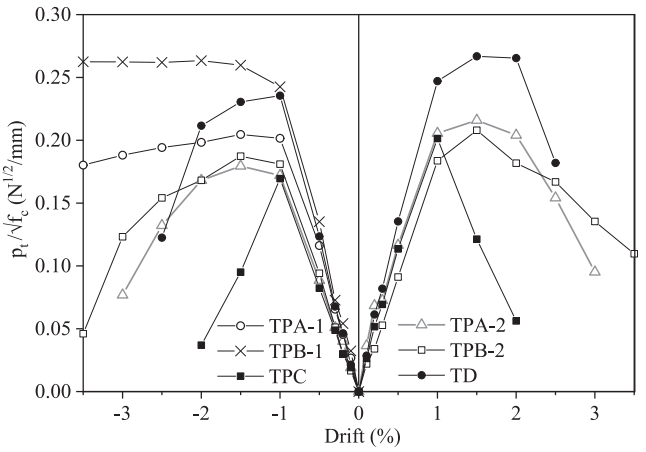

Fig. 12. Principal tensile stresses, p_t, normalized by $\sqrt{f_c}$ (f_c in MPa).

observed in specimens TPA-1 and TPB-1, monotonically tested, were 13 % and 41 % higher than in specimens TPA-2 and TPB-2, respectively. In specimen TPC was observed a significant drop after peak while in the other specimens the slope of the envelope curves was smaller.

5. Conclusions

This paper describes an experimental campaign carried out for assessment the monotonic and cyclic behaviour of six full-scale RC exterior beam-column joints built with plain and deformed bars and without seismic reinforcement detailing. The specimens represent the typical exterior beam-column joints in existing RC structures in the European Mediterranean countries until the 1970 s. The influence of reinforcing steel surface, lapping of the longitudinal reinforcing bars in the column, anchorage of the beam longitudinal reinforcing bars in the core joint and lateral loading history (monotonic or cyclic) on the response were investigated. From the analysis of the experimental results the following conclusions can be drawn:

- The global behaviour of specimen types TPA, TPB and TD was similar in terms of maximum strength, ductility, dissipated energy and equivalent damping. However, in specimen TPC the results were different than the other specimens once a premature failure (ultimate drift of 1.4 % while for the reference specimen was 2.6 %) was observed because of the poor anchorage detailing of the beam reinforcing bars in the core joint that induced the concrete wedge mechanism. Therefore, the anchorage detailing has an important role on the joint cyclic behaviour and it may compromise the response of the RC structure.
- At drift demand of 2.5 %, specimen TD dissipated more 21 % and 43 % than specimens TPA-2 and TPB-2, respectively. These differences are related with the better bond conditions (presence of deformed reinforcing bars) in the specimen TD that spread the damage over the element's length. Moreover, at ultimate drift specimen TD (with deformed bars) had more 19 % of equivalent damping than specimen TPA-2 (with plain bars).
- The methodology adopted to compute the energy dissipated by the components (joint, columns and beam) represents in average 94 % of the total experimental dissipated energy (coefficient of variance equals to 16 %). Therefore, the adopted methodology can estimate the dissipated energy of each component with accuracy. The beam had dissipated more energy than the sum of columns and joint. The joint was the element that dissipate less energy.
- Shear joint failure was observed for all specimens, except for specimens with lapping of the longitudinal bars in the superior column. The shear failure was a consequence of non-transversal reinforcement in the core joint and it justify the important of improve the joint concrete confinement during strengthening interventions in RC structures.
- The nominal horizontal joint shear stress and corresponding horizontal shear force limits of *ACI* 369.1M-17 [39] were adequate for the exterior beam-column joints here studied. The joint shear limit of the EC8-1 was almost twice the maximum horizontal shear force observed in the tests. This justify that the procedure presents in EC8-1 may not be adopted in EC8-3 for seismic assessment of RC beam-column joints.

CRediT authorship contribution statement

José Melo: Conceptualization, Methodology, Funding acquisition, Data curation, Formal analysis, Writing - original draft, Writing - review & editing. **Humberto Varum:** Conceptualization, Supervision, Writing - review & editing. **Tiziana Rossetto:** Conceptualization, Supervision, Writing - review & editing.

Declaration of Competing Interest

The authors declare that they have no known competing financial interests or personal relationships that could have appeared to influence the work reported in this paper.

Data availability

Data will be made available on request.

Acknowledgments

This paper reports research developed under financial support provided by "FCT - Fundação para a Ciência e Tecnologia", Portugal, co-funded by the European Social Fund, namely through the post-doc fellowship of the first author, with reference SFRH/BPD/115352/2016 and by Base Funding - UIDB/04708/2020 and Programmatic Funding - UIDP/04708/2020 of the CONSTRUCT - Instituto de I&D em Estruturas e Construções - funded by national funds through the FCT/MCTES (PIDDAC). The authors acknowledge the staff of the Civil Engineering Laboratory at the University of Aveiro for the support in the preparation and development of the testing campaign.

References

[1] Antonopoulos CP, Triantafillou TC. Experimental Investigation of FRP-Strengthened RC Beam-Column Joints. J Compos Constr 2003;7(1):39–49.
[2] Varum H. *Seismic assessment, strengthening and repair of existing buildings*. Departamento de Engenharia Civil. Aveiro: Universidade de Aveiro; 2003.
[3] Rodrigues H, et al. Experimental evaluation of rectangular reinforced concrete column behaviour under biaxial cyclic loading. Earthquake Eng Struct Dyn 2013; 42(2):239–59.
[4] Rodrigues H, et al. A comparative analysis of energy dissipation and equivalent viscous damping of RC columns subjected to uniaxial and biaxial loading. Eng Struct 2012;35:149–64.
[5] Fardis MN. *Seismic Design, Assessment and Retrofitting of Concrete Buildings, based on EN-Eurocode 8*. Geotechnical, Geological, and Earthquake Engineering, vol. 8. Springer, Dordrecht; 2009. p. 744.
[6] I. Press. Guidelines for Displacement-based Design of Buildings and Bridges. In: LESSLOSS - Risk Mitigation for Earthquakes and Landslides; 2007.
[7] Melo J, et al. Numerical modelling of the cyclic behaviour of RC elements built with plain reinforcing bars. Eng Struct 2011;33:273–86.
[8] Fernandes C, et al. Cyclic Behavior of Substandard Reinforced Concrete Beam-Column Joints with Plain Bars. ACI Struct J 2013;110(1):137–47.
[9] Liu A, Park R. Seismic behavior and retrofit of pre-1970's as-built exterior beam-column joints reinforced by plain round bars. Bull New Zealand Soc Earthquake Eng 2001;34(1):68–81.
[10] Fernandes C et al. *Cyclic behavior of a two-span RC beam built with plain reinforcing bars*. Budapest University of Technology and Economics; 2011.
[11] Ludovico MD, et al. Cyclic Behavior of Nonconforming Full-Scale RC Columns. J Struct Eng 2014;140(5):04013107.

[12] Braga F, Gigliotti R, Laterza M. R/C Existing Structures with Smooth Reinforcing Bars: Experimental Behaviour of Beam-Column Joints Subject to Cyclic Lateral Loads. Open Construct Build Technol J 2009;3:52–67.
[13] Ricci P, et al. Experimental tests of unreinforced exterior beam–column joints with plain bars. Eng Struct 2016;118:178–94.
[14] De Risi MT, Verderame GM. Experimental assessment and numerical modelling of exterior non-conforming beam-column joints with plain bars. Eng Struct 2017;150:115–34.
[15] Verderame GM, De Risi MT, Ricci P. Experimental Investigation of Exterior Unreinforced Beam-Column Joints with Plain and Deformed Bars. J Earthquake Eng 2018;22(3):404–34.
[16] Gaetano R, Margherita P. Seismic Behavior of Exterior Beam-Column Connections with Plain Bars and Effects of Upgrade. ACI Struct J 2012;109(2).
[17] Bousias S, Spathis A-L, Fardis MN. Seismic Retrofitting of Columns with Lap Spliced Smooth Bars Through FRP or Concrete Jackets. J Earthquake Eng 2007;11(5):653–74.
[18] Esmaeeli E, et al. Assessment of the efficiency of prefabricated hybrid composite plates (HCPs) for retrofitting of damaged interior RC beam–column joints. Compos Struct 2015;119:24–37.
[19] Pohoryles DA, et al. Experimental Comparison of Novel CFRP Retrofit Schemes for Realistic Full-Scale RC Beam-Column Joints. J Compos Constr 2018;22(5):04018027.
[20] Vecchio CD, et al. Seismic Retrofit of Real Beam-Column Joints Using Fiber-Reinforced Cement Composites. J Struct Eng 2018;144(5):04018026.
[21] Shoukry ME, Tarabia AM, Abdelrahman MZ. Seismic retrofit of deficient exterior RC beam-column joints using steel plates and angles. Alexandria Eng J 2022;61(4):3147–64.
[22] Tavasoli E, Rezaifar O, Kheyroddin A. Seismic performance of RC joints retrofitted by external diagonal bolts. J Build Eng 2022;46:103691.
[23] Li Y, Sanada Y. Seismic strengthening of existing RC beam-column joints by wing walls. Earthquake Eng Struct Dyn 2017;46(12):1987–2008.
[24] Golias E, et al. Application of X-Shaped CFRP Ropes for Structural Upgrading of Reinforced Concrete Beam-Column Joints under Cyclic Loading-Experimental Study. Fibers 2021;9(7):42.
[25] Governo DD. *Regulamento do Betão Armado (RBA), Decreto n.° 25948, 16 de Outubro, serie I, num.* Lisbon; 1935. p. 240.
[26] Governo DD. Regulamento de Estruturas de Betao Armado, Decreto n.° 47723, 20 de Maio, serie I, num. Diário do Governo: Lisbon; 1967. p. 119.
[27] CEN. *Eurocode 2: Design of concrete structures - Part 1-1: General rules and rules for buildings*, CEN, Editor. Brussels: Eupean Comitee for Standardization; 2004. p. 226.
[28] CEN, EN ISO 6892-1:2009 - Metallic materials - Tensile testing - Part 1: Method of test at room temperature. Brussels; 2009.
[29] Park YJ, Ang AHS, Wen YK. Damage-limiting aseismic design of buildings. Earthquake Spectra 1987;3(1).
[30] Melo J, Varum H, Rossetto T. Experimental cyclic behaviour of RC columns with plain bars and proposal for Eurocode 8 formula improvement. Eng Struct 2015;88:22–36.
[31] CEN, EN 1998-1:2004+A1 - Eurocode 8: Design of structures for earthquake resistance - Part 1: General rules, seismic actions and rules for buildings. CEN: Brussels; 2013.
[32] Melo J, Varum H, Rossetto T. Cyclic behaviour of interior beam–column joints reinforced with plain bars. Earthquake Eng Struct Dyn 2015;44(9):1351–71.
[33] Priestley MJN. Myths and Fallacies in Earthquake Engineering, Revisited" The Mallet Milne Lecture. Pavia, Italy: IUSS Press; 2003.
[34] Shiohara H. New Model for Shear Failure of RC Interior Beam-Column Connections. J Struct Eng 2001;127(2):152–60.
[35] Tsonos AG. Cyclic Load Behavior of Reinforced Concrete Beam-Column Subassemblages of Modern Structures. ACI Struct J 2007;104(4):468–78.
[36] Shigeru Hakuto RP, Tanaka H. Seismic Load Tests on Interior and Exterior Beam-Column Joints with Substandard Reinforcing Details. ACI Struct J 2000;97(1).
[37] Hwang S-J, Lee H-J. Analytical Model for Predicting Shear Strengths of Exterior Reinforced Concrete Beam-Column Joints for Seismic Resistance. ACI Struct J 1999;96(5).
[38] CEN, NP EN 1998-3. Eurocode 8, Design of structures for earthquake resistance - Part 3: Assessment and retrofitting of buildings. European Committee for Standardization: Brussels, Belgium; 2005.
[39] Institute AC. *Standard Requirements for Seismic Evaluation and Retrofit of Existing Concrete Buildings (ACI 369.1M-17) and Commentary*. Farmington Hills; 2018.
[40] Institute AC. Building Code Requirements for Structural Concrete (ACI 318–19). Farmington Hills: American Concrete Institute; 2019.
[41] Chalioris CE, Favvata MJ, Karayannis CG. Reinforced concrete beam–column joints with crossed inclined bars under cyclic deformations. Earthquake Eng Struct Dyn 2008;37(6):881–97.